Effective dielectric constant of periodic composite structures

S. Datta, C. T. Chan, K. M. Ho, and C. M. Soukoulis
Ames Laboratory and Department of Physics and Astronomy, Iowa State University, Ames, Iowa 50011
(Received 25 June 1993)

Using a plane-wave-expansion method, we obtained expressions for the effective dielectric constants of composite periodic dielectric materials as the long-wavelength limit of the photonic-band-structure problem. The effective dielectric constants of several classes of photonic-band-gap structures are computed and we found that in the long-wavelength limit, they can be isotropic, uniaxial, or biaxial, depending on the symmetry of the structure under consideration. We also found that the scalar wave approximation gives poor results for effective dielectric constants while the Maxwell-Garnett theory offers very good approximations in the low-filling-ratio regimes.

I. INTRODUCTION

The propagation of electromagnetic waves in the long-wavelength limit of heterogeneous media is an old but still very active subject.[1] Initially, various effective medium approaches like the Maxwell-Garnett approximation[2] were used to determine the dielectric constant and other properties in the long-wavelength limit. It was later realized that these were inadequate and that the microgeometry of the medium needs to be taken into account even though it is on a much smaller scale than the probing wavelength. Several such studies were made by McPhedran and McKenzie[3] and others for periodic systems using the boundary-matching approach. The efficacy of this approach is limited to special shapes like spheres and cubes which do not overlap. In recent years several[4–6] groups have used Fourier expansion techniques which can be used to study any periodic microgeometry and are therefore much wider in scope than the previous efforts. Very recently, there has been a great deal of interest in the photonic-band-gap problem.[7–13] It has been proposed that a heterogeneous medium composed of periodic arrangements of low loss dielectric material can have a frequency gap in which no electromagnetic wave can propagate in any direction, analogous to the electronic band gap for Bloch electron waves in a periodic lattice of ion cores. Such a frequency gap is frequently called a "photonic band gap" (PBG), while those periodic dielectric materials that may have a photonic band gap are now frequently called photonic-band-gap materials in the literature. In this paper, we will use the term "PBG material" in its broader sense to refer to heterogenous media with periodic arrangements of one type of material embedded in another. Exciting physical phenomena and possible industrial applications have been proposed if such a photonic band gap does exist.[13] It was later discovered[7–9] that the realization of a bona-fide photonic band gap in three dimensions is much more difficult than originally purported. Nevertheless, it has now been demonstrated both theoretically[9–12] and experimentally[13] that full three-dimensional photonic band gaps can be realized in certain classes of periodic dielectric materials. The recent thrust in this area is partly fueled by advances in theoretical techniques, which allow us to solve the vector electromagnetic wave equations in a periodic medium and thus making the design of photonic-band-gap materials possible within current computation capabilities. The plane wave expansion method is by far the most popular theoretical tool for studying the photonic-band-gap problem and this Fourier space technique is similar in spirit to the methods of Tao, Chen, and Sheng[4] and Shen *et al.*,[5] although the latter focused their attention solely on the $k \to 0$ limit. It is interesting to note that a few authors[8,12] who worked on the photonic-band-gap problem have also studied the effective dielectric constant, but the effective dielectric constant is obtained by finite differences as slope of the photonic-band dispersion at a small k in a certain propagation direction. We will show that the photonic-band-structure problem (arbitrary but nonzero k) and the effective dielectric constant ($k \to 0$ limit) can be solved in the same problem, and we obtained formally closed-form expressions for the dielectric constant as the $k \to 0$ limit of the photonic band structure. Using this method, we calculated the effective dielectric constant of several classes of photonic-band-gap materials. It is interesting to note that besides the possibility of possessing photonic gaps, some of these materials are also optically anisotropic and thus will exhibit sizable birefringence.

II. THE LONG-WAVELENGTH LIMIT

For the class of PBG materials we are interested in, the most straightforward approach to studying the electromagnetic (EM) spectrum is to operate in the Fourier space, where the periodic boundary condition can be put in trivially by imposing Bloch's theorem and there is no restriction on the shape of the structural units as long as they are in a periodic formation. We thus solve the wave equation by expanding the dielectric constant of the periodic structure in plane waves of the form $e^{i\mathbf{G}\cdot\mathbf{r}}$ where the $\mathbf{G}$'s are the reciprocal lattice vectors as determined by the periodicity of the system. This transforms the Maxwell equations into a matrix equation which, upon

0163-1829/93/48(20)/14936(8)/$06.00

diagonalization, gives the frequency and the eigenvectors of the EM wave eigenmodes. This has recently been, with slight variations, the favorite approach of many authors.[7–12] The same approach can also be used to find the long-wavelength limit of the EM dispersion curves and thus determine the effective dielectric constant of periodic composite materials. One obvious way is simply to use finite differences, where the effective dielectric constant can be deduced from the slope of the EM wave dispersion curves as $|k| \to 0$. What we are presenting here is an alternate approach in which we deduce the effective dielectric constant via perturbation theory. For EM waves with frequency ω, the Maxwell equations can be written as

$$\nabla \cdot \mathbf{D} = 0 ,$$

$$\nabla \times \mathbf{H} = -i\frac{\omega}{c}\mathbf{D} ,$$

$$\nabla \times \mathbf{E} = i\frac{\omega}{c}\mathbf{H} ,$$

$$\nabla \cdot \mathbf{H} = 0 , \tag{1}$$

and

$$\mathbf{D}(\mathbf{r}) = \epsilon(\mathbf{r})\mathbf{E}(\mathbf{r}) , \tag{2}$$

where $\epsilon(\mathbf{r})$ is a real and periodic function of $\mathbf{r}$ and frequency independent in the range of frequency under consideraton. We also take the magnetic permeability $\mu = 1$. Since $\epsilon(\mathbf{r})$ is periodic, we can use Bloch's theorem to expand the $\mathbf{H}$, $\mathbf{E}$, and $\mathbf{D}$ fields, for example,

$$\mathbf{E}(\mathbf{r}) = \sum_{\mathbf{K}} \mathbf{E}_{\mathbf{K}} e^{i\mathbf{K}\cdot\mathbf{r}} , \tag{3}$$

where $\mathbf{K} = \mathbf{k} + \mathbf{G}$, with $\mathbf{k}$ being a wave vector (in the Brillouin zone) that determines the propagation direction and wavelength of the EM wave, and $\mathbf{G}$ is a reciprocal lattice vector. Equation (2) and the corresponding expansions for $\mathbf{E}$ and $\mathbf{D}$ transform the Maxwell equations (1) into

$$\mathbf{K} \cdot \mathbf{D}_{\mathbf{K}} = 0 ,$$

$$\mathbf{K} \times \mathbf{H}_{\mathbf{K}} = -\frac{\omega}{c}\mathbf{D}_{\mathbf{K}} ,$$

$$\mathbf{K} \times \mathbf{E}_{\mathbf{K}} = \frac{\omega}{c}\mathbf{H}_{\mathbf{K}} ,$$

$$\mathbf{K} \cdot \mathbf{H}_{\mathbf{K}} = 0 . \tag{4}$$

We can now eliminate the $\mathbf{H}$ field in terms of the $\mathbf{E}$ field, and get

$$\mathbf{K} \times \mathbf{K} \times \mathbf{E}_{\mathbf{K}} = -\frac{\omega^2}{c^2} \sum_{\mathbf{K}'} \epsilon_{\mathbf{K}\mathbf{K}'} \mathbf{E}_{\mathbf{K}'} . \tag{5}$$

We decompose the Fourier components $\mathbf{E}_{\mathbf{K}}$ into longitudinal and transverse components

$$\mathbf{E}_{\mathbf{K}} = e_{\mathbf{K}}\hat{\mathbf{K}} + e_{\mathbf{x}_{\mathbf{K}}}\hat{\mathbf{x}}_{\mathbf{K}} + e_{\mathbf{y}_{\mathbf{K}}}\hat{\mathbf{y}}_{\mathbf{K}} , \tag{6}$$

where $(\hat{\mathbf{x}}_{\mathbf{K}}, \hat{\mathbf{y}}_{\mathbf{K}}, \hat{\mathbf{K}})$ form an orthogonal triad and $e_{\mathbf{K}}, e_{\mathbf{x}_{\mathbf{K}}}, e_{\mathbf{y}_{\mathbf{K}}}$ are the $\mathbf{E}$ field components along these directions.

Putting Eq. (6) into Eq. (5) and forming dot products with $\hat{\mathbf{K}}$ and $(\hat{\mathbf{x}}_{\mathbf{K}}, \hat{\mathbf{y}}_{\mathbf{K}})$, respectively, we obtain

$$0 = \sum_{\mathbf{K}'} \epsilon_{\mathbf{K}\mathbf{K}'} \left[\left(\hat{\mathbf{K}} \cdot \hat{\mathbf{K}}'\right) e_{\mathbf{K}'} + \left(\hat{\mathbf{K}} \cdot \hat{\mathbf{x}}_{\mathbf{K}'}\right) e_{\mathbf{x}_{\mathbf{K}'}} + \left(\hat{\mathbf{K}} \cdot \hat{\mathbf{y}}_{\mathbf{K}'}\right) e_{\mathbf{y}_{\mathbf{K}'}} \right] \tag{7}$$

and

$$K^2 \begin{bmatrix} e_{\mathbf{x}_{\mathbf{K}}} \\ e_{\mathbf{y}_{\mathbf{K}}} \end{bmatrix} = \frac{w^2}{c^2} \sum_{\mathbf{K}'} \left\{ \epsilon_{\mathbf{K}\mathbf{K}'} \begin{bmatrix} \hat{\mathbf{x}}_{\mathbf{K}} \cdot \hat{\mathbf{x}}_{\mathbf{K}'} & \hat{\mathbf{y}}_{\mathbf{K}} \cdot \hat{\mathbf{y}}_{\mathbf{K}'} \\ \hat{\mathbf{y}}_{\mathbf{K}} \cdot \hat{\mathbf{x}}_{\mathbf{K}'} & \hat{\mathbf{y}}_{\mathbf{K}} \cdot \hat{\mathbf{y}}_{\mathbf{K}'} \end{bmatrix} \begin{bmatrix} e_{\mathbf{x}_{\mathbf{K}'}} \\ e_{\mathbf{y}_{\mathbf{K}'}} \end{bmatrix} + \epsilon_{\mathbf{K}\mathbf{K}'} \begin{bmatrix} \left(\hat{\mathbf{x}}_{\mathbf{K}} \cdot \hat{\mathbf{K}}'\right) e_{\mathbf{K}'} \\ \left(\hat{\mathbf{y}}_{\mathbf{K}} \cdot \hat{\mathbf{K}}'\right) e_{\mathbf{K}'} \end{bmatrix} \right\} . \tag{8}$$

If we define

$$(\epsilon_{LL})_{\mathbf{K}\mathbf{K}'} = \epsilon_{\mathbf{K}\mathbf{K}'} \left(\hat{\mathbf{K}} \cdot \hat{\mathbf{K}}'\right) ,$$

$$(\epsilon^{\alpha}_{LT})_{\mathbf{K}\mathbf{K}'} = \epsilon_{\mathbf{K}\mathbf{K}'} \left(\hat{\mathbf{K}} \cdot \hat{\alpha}_{\mathbf{K}'}\right)$$

(the subscripts L and T stand for longitudinal and transverse, respectively, and $\alpha = x$ or y), then eliminating the longitudinal components $e_{\mathbf{K}'}$ in Eqs. (7) and (8) leads to

$$K^2 \begin{bmatrix} e_{\mathbf{x}_{\mathbf{K}}} \\ e_{\mathbf{y}_{\mathbf{K}}} \end{bmatrix} = \frac{\omega^2}{c^2} \sum_{\mathbf{K}'} \left\{ \begin{pmatrix} \epsilon^{xx}_{TT} & \epsilon^{xy}_{TT} \\ \epsilon^{y}_{TT} & \epsilon^{yy}_{TT} \end{pmatrix} - \begin{pmatrix} \epsilon^{x}_{TL}\epsilon^{-1}_{LL}\epsilon^{x}_{LT} & \epsilon^{x}_{TL}\epsilon^{-1}_{LL}\epsilon^{y}_{LT} \\ \epsilon^{y}_{TL}\epsilon^{-1}_{LL}\epsilon^{x}_{LT} & \epsilon^{y}_{TL}\epsilon^{-1}_{LL}\epsilon^{y}_{LT} \end{pmatrix} \right\} \begin{bmatrix} e_{\mathbf{x}_{\mathbf{K}'}} \\ e_{\mathbf{y}_{\mathbf{K}'}} \end{bmatrix} , \tag{9}$$

where

$$\left(\epsilon_{TT}^{\alpha\beta}\right)_{\mathbf{K}\mathbf{K}'} = \epsilon_{\mathbf{K}\mathbf{K}'}\hat{\alpha}_{\mathbf{K}} \cdot \hat{\beta}_{\mathbf{K}'} \quad (\alpha, \beta = x, y) .$$

Equation (9) can be solved to obtain the photon band structure, although the corresponding equations for the **H** field[9] is more straightforward to solve numerically. However, Eq. (9) has the advantage that we can obtain the long-wavelength limit $|k| \to 0$ in a straightforward way. We can write Eq. (9) as **(K=k+G)**,

$$(\mathbf{k}+\mathbf{G})^2 \mathbf{E}_{\mathbf{k}+\mathbf{G}}^T = \frac{\omega^2}{c^2} \sum_{\mathbf{G}'} \xi_{\mathbf{k}+\mathbf{G},\mathbf{k}+\mathbf{G}'} \mathbf{E}_{\mathbf{k}+\mathbf{G}'}^T , \qquad (10)$$

where the transverse **E** field is defined as

$$\mathbf{E}_{\mathbf{k}+\mathbf{G}}^T = \begin{bmatrix} e_{\mathbf{x}_{\mathbf{k}+\mathbf{G}}} \\ e_{\mathbf{y}_{\mathbf{k}+\mathbf{G}}} \end{bmatrix} .$$

At the long-wavelength limit, the effective dielectric constant $\epsilon_{k\to 0}$ is defined by $\epsilon_{\text{eff}}\omega^2 = c^2k^2$. So Eq. (10) becomes

$$\mathbf{E}_{\mathbf{k}+\mathbf{G}}^T = \frac{\omega^2}{c^2k^2}\left(\frac{k^2}{[\mathbf{k}+\mathbf{G}]^2}\right)\sum_{\mathbf{G}'} \xi_{\mathbf{k}+\mathbf{G},\mathbf{k}+\mathbf{G}'}\mathbf{E}_{\mathbf{k}+\mathbf{G}'}^T$$

$$= \epsilon_{\text{eff}}^{-1}\left(\frac{k^2}{[\mathbf{k}+\mathbf{G}]^2}\right)\sum_{\mathbf{G}'} \xi_{\mathbf{k}+\mathbf{G},\mathbf{k}+\mathbf{G}'}\mathbf{E}_{\mathbf{k}+\mathbf{G}'}^T . \qquad (11)$$

Now taking the $k \to 0$ limit, all $\mathbf{G} \neq 0$ components of $\mathbf{E}_{\mathbf{k}+\mathbf{G}}^T$ die off as $1/G^2$.

Therefore only the first term in the right hand side of Eq. (11) survives and $\mathbf{E}_{k\to 0,\mathbf{G}=\mathbf{0}}^T = \epsilon_{\text{eff}}^{-1}\xi_{00}\mathbf{E}_{k\to 0,\mathbf{G}=\mathbf{0}}^T$. Thus

$$\epsilon_{\text{eff}} = \xi_{00} = \left[\begin{pmatrix} \epsilon_{TT}^{xx} & \epsilon_{TT}^{xy} \\ \epsilon_{TT}^{yx} & \epsilon_{TT}^{yy} \end{pmatrix} - \begin{pmatrix} \epsilon_{TL}^x\epsilon_{LL}^{-1}\epsilon_{LT}^x & \epsilon_{TL}^x\epsilon_{LL}^{-1}\epsilon_{LT}^y \\ \epsilon_{TL}^y\epsilon_{LL}^{-1}\epsilon_{LT}^x & \epsilon_{TL}^y\epsilon_{LL}^{-1}\epsilon_{LT}^y \end{pmatrix}\right]_{\mathbf{G}=0,\mathbf{G}'=0} , \qquad (12)$$

where $(\epsilon_{TT}^{\alpha\beta})_{\mathbf{k}\mathbf{k}'} = \epsilon_{\mathbf{k}\mathbf{k}'}\hat{\alpha_{\mathbf{k}}} \cdot \hat{\beta_{\mathbf{k}'}}$, $(\epsilon_{LL})_{\mathbf{k}\mathbf{k}'} = \epsilon_{\mathbf{k}\mathbf{k}'}(\hat{\mathbf{k}} \cdot \hat{\mathbf{k}'})$, $(\epsilon_{TL}^x)_{\mathbf{k}\mathbf{k}'} = (\epsilon_{\mathbf{k}\mathbf{k}'})(\hat{\mathbf{x}_{\mathbf{k}}} \cdot \hat{\mathbf{k}'})$, and $(\hat{\alpha_{\mathbf{k}}}, \hat{\beta_{\mathbf{k}}}, \hat{\mathbf{k}})$ form an orthogonal triad, and $\epsilon_{\mathbf{k}\mathbf{k}'} = \frac{1}{\Omega}\int e^{i(\mathbf{k}-\mathbf{k}')\cdot\mathbf{r}}\epsilon(\mathbf{r}) = \frac{1}{\Omega}\int e^{i(\mathbf{G}-\mathbf{G}')\cdot\mathbf{r}}\epsilon(\mathbf{r})$ is the Fourier transform of the dielectric function.

Noting that $(\epsilon_{TT}^{xy})_{\mathbf{G}=0,\mathbf{G}'=0}$ is by definition zero, the first term at $\mathbf{G} = 0$ and $\mathbf{G}' = 0$ becomes

$$\begin{pmatrix} \epsilon_{TT}^{xx} & \epsilon_{TT}^{xy} \\ \epsilon_{TT}^{yx} & \epsilon_{TT}^{yy} \end{pmatrix} = \begin{pmatrix} \langle\epsilon\rangle & 0 \\ 0 & \langle\epsilon\rangle \end{pmatrix} , \qquad (13)$$

where

$$\langle\epsilon\rangle = (1-f)\epsilon_1 + f\epsilon_2 = \epsilon_1[1 + (\Delta\epsilon/\epsilon_1)f] , \qquad (14)$$

which is the scalar wave result for a periodic array of material of dielectric constant ϵ_2 embedded in material of dielectric constant ϵ_1 with a filling ratio f. The diagonalization of the 2×2 matrix in the second term gives the correction to the scalar wave result. Since it is a 2×2 matrix, there are in general two effective dielectric constants (with two corresponding wave velocities) in a general direction of propagation. For the special case of a cubic crystal Eq. (12) reduces to

$$\tilde{\epsilon}_{\text{eff}} = \begin{pmatrix} \langle\epsilon\rangle & 0 \\ 0 & \langle\epsilon\rangle \end{pmatrix} + \begin{pmatrix} \alpha & 0 \\ 0 & \alpha \end{pmatrix} , \qquad (15)$$

where $\alpha = \epsilon_{TL}^x\epsilon_{LL}^{-1}\epsilon_{LT}^x$. In this case, there is only one wave velocity in all directions.

The most computationally intensive part in the evaluation of Eqs. (12) and (15) lies in the computation of ϵ_{LL}^{-1}. If we use N plane waves in the expansion Eq. (3) ϵ_{LL}^{-1} is the inverse of a $N \times N$ matrix. Although Eq. (12) is formally "exact" there is always a truncation error associated with truncating the Fourier series. The size of the matrix required to obtain reasonably converged results depends on the dielectric contrast (higher contrast requiring more plane waves) as well as the geometric arrangement of "objects." Usually spheres that are nearly touching require a large number of plane waves to converge.[12] Convergence tests for some particular cases are given in the Appendix, where we also discuss another way of obtaining the effective dielectric constant that may be more efficient in some situations.

III. NUMERICAL RESULTS

Using the above method, we have calculated the effective dielectric constant in the long-wavelength limit for a few prototypical PBG materials, which consist of a periodic array of a material of a specific dielectric constant embedded in a uniform matrix of a different dielectric contrast. The structures we considered include spheres arrayed in face-centered cubic, simple cubic, and diamond structures. We considered the case with material spheres embedded in air as well as the conjugate configuration of air spheres embedded in materials of high refractive index. Different filling ratios are considered. The dielectric contrast is set at 13.0, which is roughly that of Si in air at optical wavelengths.

We note that the formulations developed in the preceding section are applicable to multicomponent systems and also systems with continuously varying dielectric constant, as long as $\epsilon(\mathbf{r})$ is periodic, although we will limit ourselves to two component systems in the following numerical computations. The results for the material spheres (Fig. 1) and air spheres (Fig. 2) are compared with the scalar wave results (which ignore the vector nature of light) and the Maxwell-Garnett theory (basically a Clausius-Mosotti relation), which is given by

$$\epsilon = \epsilon_1\left(\frac{2\epsilon_1 + \epsilon_2 + 2f(\epsilon_2 - \epsilon_1)}{2\epsilon_1 + \epsilon_2 - f(\epsilon_2 - \epsilon_1)}\right) . \qquad (16)$$

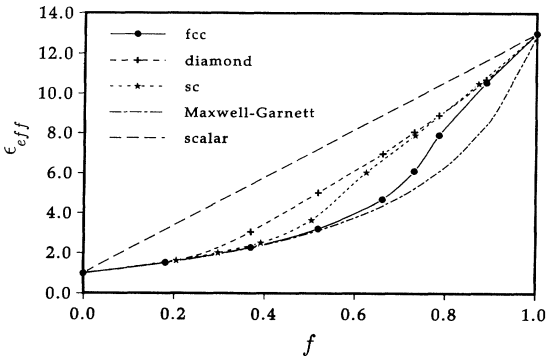

FIG. 1. The effective dielectric constant ϵ_{eff} for the fcc, sc, and diamond structures composed of material spheres (dielectric constant $\epsilon = 13$) in air background as a function of the filling ratio f compared with the scalar and Maxwell-Garnett results.

We observe that the effective dielectric constant is smaller than the scalar wave result in all the cases we have considered and also that it is different for different structures. For the scalar wave result, the effective dielectric constant is independent of the microstructure of the media, and is determined entirely by the volume averaged dielectric constant of the media. What this means is that the scalar wave provides no information whatever about the structure in the long-wavelength limit. However, the vector nature of the EM waves allows some sensitivity to the microstructure of the media even as $|k| \to 0$ so that, for the same filling ratio, the effective dielectric constant changes with the structure factor of the material under consideration. We note that for the cubic systems under consideration, the term α in Eq. (15) can be written in the form of a formal series expansion in $\Delta\epsilon/\epsilon_1$ (we take $\epsilon_1 > \epsilon_2$). Then

$$\tilde{\epsilon}_{k\to 0} = \epsilon_1 \Bigg[1 + (\Delta\epsilon/\epsilon_1) f - (\Delta\epsilon/\epsilon_1)^2 \sum_{\mathbf{G}} \mathcal{S}^2(\mathbf{G})(\hat{\mathbf{x}}\cdot\mathbf{G})^2 + \cdots \Bigg] , \quad (17)$$

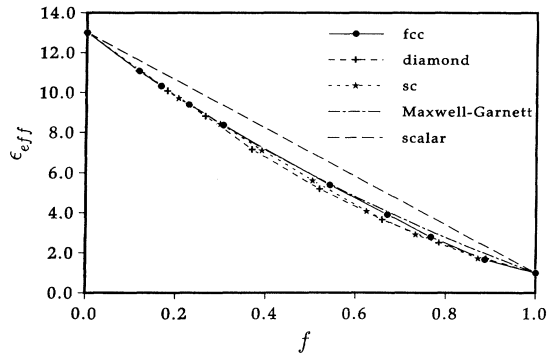

FIG. 2. The effective dielectric constant ϵ_{eff} for the fcc, sc, and diamond structures composed of air spheres in dielectric background (dielectric constant $\epsilon = 13$) as a function of the filling ratio f compared with the scalar and Maxwell-Garnett results.

where $\mathcal{S}(\mathbf{G}) = \frac{1}{\Omega}\sum_\tau \exp(i\mathbf{G}\cdot\tau)\mathbf{F}(\mathbf{G})$ is the structure factor of the composite material in Fourier space, and $\mathbf{F}(\mathbf{G})$ is the Fourier transform of the function $\mathbf{F}(\mathbf{r})$ which takes the value of 1 in the regions with dielectric constant ϵ_2 and zero at regions with dielectric constant ϵ_1. This expansion can be obtained by expanding ϵ_{LL}^{-1} in a series of matrices. For multicomponent systems, we can obtain a similar expression if we expand about the volume-averaged dielectric constant. Although this expression is not practical for numerical computations except for very small dielectric constant contrasts, it does give us more insight than Eq. (15). We note that the term up to $\Delta\epsilon/\epsilon_1$ is precisely the scalar wave result, which shows no sensitivity to the microstructure of the composite system. The leading $(\Delta\epsilon/\epsilon_1)^2$ correction term to the scalar result is negative definite, so that it is quite natural that all the effective dielectric constants are smaller than the scalar wave result. The structure factor and the vector nature of EM waves enter the expression at this order. It is also interesting to compare the present results with those obtained from the Maxwell-Garnett (MG) expression. For both the material-in-air and air-in-material configurations, the MG results are in general better approximations than the scalar wave results. The scalar wave approximation to the vector wave equations has been used previously to study the photonic-band-gap problem. We now know that it can give qualitatively different results regarding the existence of photonic band gaps and also give rather poor approximations to the long-wavelength effective dielectric constants. In the regime of small filling ratios, the MG results agree well with the vector-wave results. This is not surprising since the MG theories are intended for small isolated spheres embedded in a medium. As we consider the different arrangement of spheres, we observe that the agreement between vector-wave results and MG results begins to deteriorate at a fairly small filling ratio for the diamond structure while the agreement remains good for a much higher filling ratio in the fcc structure. The simple cubic structure lies in between. This is because the filling ratio corresponding to the condition of touching spheres increases in the order diamond, simple cubic, and fcc. We also note from Figs. 1 and 2 that the MG results constitute a lower bound for the material-in-air and an upper bound for the air-in-material configurations. Notice that the MG results agree reasonably well with our numerical results for air spheres (Fig. 2) for almost all the filling ratios f.

The optical properties of crystals in nature can be classified into three groups: isotropic, uniaxial, and biaxial, depending on the symmetry of the crystal. Amorphous materials and crystals of cubic symmetry have the same values for all three principal refractive indices. The index ellipsoid is a sphere and there is only one effective wave velocity in all directions. For crystal systems with lower symmetries, such as trigonal, tetragonal, or hexagonal, two of the principal refractive indices are equal (usually called ordinary) and the third refractive index (extraordinary) is different. The index ellipsoid is a spheroid in this case. There are two different wave velocities in a general direction of propagation. In those crystals with even

lower symmetry, such as monoclinic, all three refractive indices are different.

The PBG materials, as far as optical properties are concerned, may be viewed as man-made "crystals." PBG structures that have the cubic symmetry, such as the dielectric balls arranged in fcc, sc, and diamond structures we have considered, are optically isotropic in the long-wavelength limit. There is only one effective dielectric constant and the effective wave velocities in all directions are the same. In the photonic band structure, the frequency vs wave vector dispersion curve should be doubly degenerate near Γ, and has the same slope in all directions.

A more interesting example is the Yablonovitch-Leung "three-cylinder" structure[13] that has been fabricated in both the microwave and micrometer length scales. The structure is fabricated by drilling three cylinders through each hole of a triangular array at an angle of 35.26° away from the normal and spread out 120° on the azimuth. This structure can be viewed as a fcc structure with nonspherical elongated atoms, or alternatively, as a "degraded" diamond structure (drilling three more sets of cylinders can create a structure of diamond symmetry). This structure is of great interest since it has been demonstrated both experimentally and theoretically that it possesses a full photonic band gap; and although the largest photonic gap that is attainable for this structure is less than that of the diamond structure, this is up to now the only geometrical structure that has been fabricated both in the microwave and micrometer length scales. Prototype of this design has also been used to improve microwave antenna performance. This structure has symmetry equivalent to a trigonal crystal and possesses 12 symmetry operations. This is thus an anisotropic structure and behaves like a uniaxial crystal in the long-wavelength limit, with the preferred axis in the [111] direction.

In Fig. 3 we have plotted $1/\sqrt{\epsilon_1}$ and $1/\sqrt{\epsilon_2}$, i.e., the effective velocities, as a function of propagation direction in the [111]–[10$\bar{1}$] plane for material cylinders (32% material) and air cylinders (21% material) in the "three-cylinder" structure with a dielectric constant ratio of 13.0. For the material cylinders, the 2×2 matrix in Eq. (12) was diagonalized to give two effective dielectric constants, and hence two effective velocities, one corresponding to the "ordinary" and the other corresponding to the "extraordinary" wave. The effective wave velocity that is the same in all directions corresponds, by definition, to the ordinary wave. We find that the two velocities coincide in the [111] direction and that the anisotropy is maximum in a direction perpendicular to it. The structure behaves like a uniaxial crystal. In fact, this case corresponds to a positive uniaxial crystal, with the ordinary wave having a higher velocity than the extraordinary wave. The conjugate structure also behaves like a positive uniaxial crystal but with less anisotropy. In principle, we need only to calculate Eq. (12) for two directions, and the extraordinary wave velocity v_e can be obtained by

$$v_{\mathbf{k}}^2 = v_o^2 \cos^2\theta + v_e^2 \sin^2\theta \ , \tag{18}$$

where v_o and v_e are the ordinary and extraordinary wave velocity, respectively, and θ is the angle between $\mathbf{k}$ and the optic axis. For the material-in-air configuration, all the points marked by dots and crosses are calculated. For the air-in-material configuration, we have calculated the effective wave velocities at [111] and [10$\bar{1}$] and the wave velocities at other angles are obtained with Eq. (18). An interesting aspect of PBG materials is that the anisotropy in the refractive index of natural crystals is dictated by nature and is usually small, while that of PBG materials can be engineered to a certain extent by man as far as technological capabilities permit. The maximum anisotropy in the refractive index $\sqrt{\epsilon}$ of a "three-cylinder" structure is plotted as a function of the filling ratio (Fig. 4) for a dielectric constant ratio of 7.0 and as a function of the dielectric constant ratio (Fig. 5) for both material-in-air and air-in-material configurations of the "three-cylinder" structure. In Fig. 5 the cylinder filling ratio is 0.32 for material cylinders and 0.85 for air cylinders. We see that quite a large anisotropy can arise by optimizing the structure.

We have considered both "material" cylinders and "air" cylinders in the "three-cylinder" structure. The commonly practiced fabrication processes involve drilling or etching and thus give air cylinder configurations. We also note that the current theory for the long-wavelength limit is applicable only to cases where the structural units

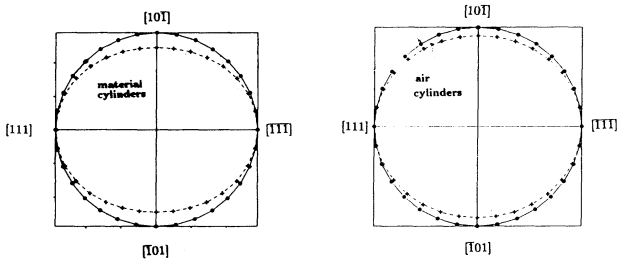

FIG. 3. The effective velocities $1/\sqrt{\epsilon_1}$ and $1/\sqrt{\epsilon_2}$ for material cylinders (32% material) and air cylinders (21% material) in the "three-cylinder" structure as a function of the propagation direction in the [111]–[10$\bar{1}$] plane. The dielectric constant ratio is 13 in both cases.

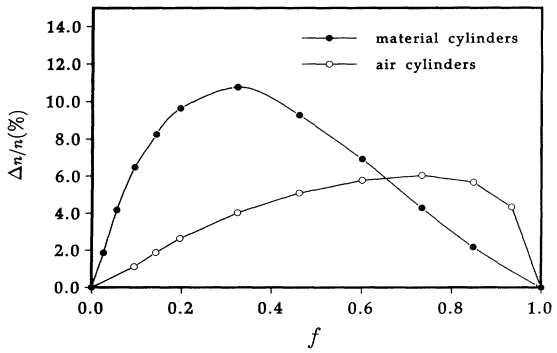

FIG. 4. The maximum anisotropy $\Delta n/n$ in the effective refractive index $n = \sqrt{\epsilon}$ of a "three-cylinder" structure plotted as a function of the filling ratio f for both material and air cylinders for material of dielectric constant $\epsilon = 7$.

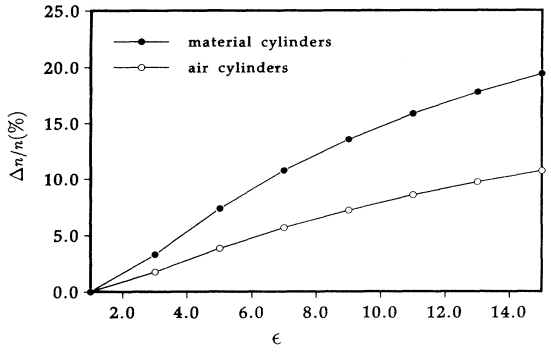

FIG. 5. The maximum anisotropy $\Delta n/n$ in the effective refractive index $n = \sqrt{\epsilon}$ of a "three-cylinder" structure plotted as a function of the dielectric constant ratio for both material (32% material) and air cylinders (15% material).

are small compared with the wavelength. For photonic-band-gap materials that are engineered to have gaps in the range of optical frequencies, the long-wavelength anisotropy described here is relevant for waves that have much lower frequencies.

For the sake of completeness, we have also considered a structure which is expected to be biaxial. The structure consists of dielectric spheres of dielectric constant $\epsilon = 13$, located at the lattice points of an orthorhombic lattice, with the lattice vectors having different lengths which are in the ratio of 1:0.833:0.714. The volume filling ratio of the spheres is 0.436. The effective velocities in the z-y, z-x, and x-y planes are plotted in Fig. 6. They do show the characteristics of a biaxial crystal.[14] The section of the normal surface in each plane consists of a circle and an ellipse, and the radii of the circles in the $x = 0$, $y = 0$, $z = 0$ planes are v_x, v_y, v_z, respectively. We found that $v_x > v_y > v_z$ because the density of scatterers is lowest in the x direction and highest in the z direction. The two optic axes are defined by the two directions in which the circle and the ellipse intersect in the z-x plane.

IV. CONCLUSION

Using the plane-wave-expansion method, we have obtained expressions for the effective dielectric constants of periodic dielectric materials. The effective dielectric constant is obtained as we consider the long-wavelength limit of the solution to the Maxwell wave equations. The present method is applicable to structures of arbitary geometrical shape as long as they form a periodic structure. Although the mathematical details are different, our approach is similar to the Fourier-space formulations of Tao, Chen, and Sheng[4] and Shen *et al.*[5]

The long-wavelength effective dielectric constants of a few composite materials were calculated and compared with the scalar wave and the Maxwell-Garnett approximation. We found that the scalar wave approximation is poor for most situations, while the Maxwell-Garnett result is good as long as the structure is composed of isolated spheres. The Maxwell-Garnett theory is not expected to be applicable to structures that support complete photonic band gaps which, as far as we know, always form percolating networks. We also found that the three-cylinder photonic-band-gap structure that has already been successfully fabricated behaves like a uniaxial system and exhibits substantial optical anisotropy. We still have to see whether such pronounced birefringence behaviors can be utilized in practice. Last, but not the least, we note that although Eqs. (12) and (A6) are formally "exact," obtaining fully converged results may be difficult for cases where the periodic structure has high dielectric contrast as the inversion of the matrix ϵ_{LL} becomes prohibitive. This is the problem shared by all Fourier-space based approaches.[4–6] If the convergence is in doubt, extrapolating to an infinite basis may help in some cases. Under such situations, the scheme recently suggested by Bergman and Dunn[6] should be the method of choice.

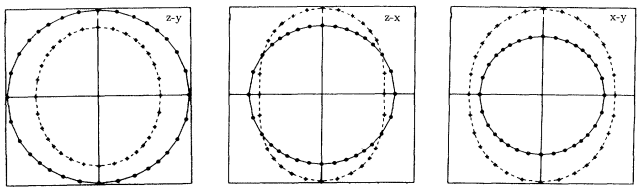

FIG. 6. The effective velocities in the z-y, z-x, and x-y planes for dielectric spheres ($\epsilon = 13.0$) in an orthorhombic "biaxial" lattice with filling ratio $f = 0.436$.

ACKNOWLEDGMENTS

Ames Laboratory is operated for the U.S. Department of Energy by Iowa State University under Contract No. W-7405-ENG-82. This work is supported by the Director of Energy Research, Office of Basic Energy Sciences, and Advanced Energy Projects including a grant of computer time on the Cray computers at NER SC at the Lawrence Livermore Laboratory.

APPENDIX

We can also obtain the effective dielectric constants using the **H** field equations [such as Eqs. (4)–(6) in Ref. 9] that we employed to solve for the photonic band dispersion relations. To obtain the photonic bands, we need to diagonalize a Hermitian matrix,

$$\sum_{\mathbf{G}',\lambda'} M^{\lambda\lambda'}_{\mathbf{k}+\mathbf{G},\mathbf{k}+\mathbf{G}'} h_{\mathbf{k}+\mathbf{G}',\lambda'} = \left(\frac{\omega}{c}\right)^2 h_{\mathbf{k}+\mathbf{G},\lambda}, \tag{A1}$$

where M is a $2N \times 2N$ matrix, with N being the number of plane waves used in the expansion, and has the form

$$M_{\mathbf{k}+\mathbf{G},\mathbf{k}+\mathbf{G}'} = |\mathbf{k}+\mathbf{G}||\mathbf{k}+\mathbf{G}'| \Phi^{\lambda\lambda'}_{\mathbf{k}+\mathbf{G},\mathbf{k}+\mathbf{G}'}$$

and

$$\Phi^{\lambda\lambda'}_{\mathbf{k}+\mathbf{G},\mathbf{k}+\mathbf{G}'} = \epsilon^{-1}_{\mathbf{G}\mathbf{G}'} \begin{bmatrix} \hat{\mathbf{y}}_{\mathbf{k}+\mathbf{G}} \cdot \hat{\mathbf{y}}_{\mathbf{k}+\mathbf{G}'} & -\hat{\mathbf{y}}_{\mathbf{k}+\mathbf{G}} \cdot \hat{\mathbf{x}}_{\mathbf{k}+\mathbf{G}'} \\ -\hat{\mathbf{x}}_{\mathbf{k}+\mathbf{G}} \cdot \hat{\mathbf{y}}_{\mathbf{k}+\mathbf{G}'} & \hat{\mathbf{x}}_{\mathbf{k}+\mathbf{G}} \cdot \hat{\mathbf{x}}_{\mathbf{k}+\mathbf{G}'} \end{bmatrix} . \tag{A2}$$

Now considering the eigenvalue value problem corresponding to the inverse of the matrix M, we have

$$\sum_{\mathbf{G}'} \frac{\Phi^{-1}_{\mathbf{k}+\mathbf{G},\mathbf{k}+\mathbf{G}'}}{|\mathbf{k}+\mathbf{G}||\mathbf{k}+\mathbf{G}'|}\psi_{\mathbf{k}+\mathbf{G}'} = \frac{c^2}{\omega^2}\psi_{\mathbf{k}+\mathbf{G}} \ . \tag{A3}$$

Multiplying both sides by k^2, we get

$$\sum_{\mathbf{G}'} \frac{k^2}{|\mathbf{k}+\mathbf{G}||\mathbf{k}+\mathbf{G}'|}\Phi^{-1}_{\mathbf{k}+\mathbf{G},\mathbf{k}+\mathbf{G}'}\psi_{\mathbf{k}+\mathbf{G}'} = \frac{k^2c^2}{\omega^2}\psi_{\mathbf{k}+\mathbf{G}} \tag{A4}$$

and specifically for the first row of this matrix equation, where $\mathbf{G} = 0$, we have

$$\left[\Phi^{-1}_{\mathbf{k},\mathbf{k}} + \sum_{\mathbf{G}'\neq 0} \frac{|\mathbf{k}|}{|\mathbf{k}+\mathbf{G}'|}\Phi^{-1}_{\mathbf{k},\mathbf{k}+\mathbf{G}'}\right]\psi_{\mathbf{k}} = \frac{k^2c^2}{\omega^2}\psi_{\mathbf{k}} \ . \tag{A5}$$

Taking the limit $k \to 0$, and noting that all but the first term on the left hand side goes to zero, we get

$$\Phi^{-1}_{00} = \lim_{k\to 0}\frac{k^2c^2}{\omega^2} = \epsilon_{\text{eff}} \ , \tag{A6}$$

so that the effective dielectric constant is just the upper-left 2×2 sub-block of the matrix Φ^{-1}. For scalar waves, $\Phi = \epsilon^{-1}$, so that we have the trivial result $\Phi^{-1}_{00} = \epsilon_{00}$. For vector waves, we may call the difference between Φ^{-1}_{00} and ϵ_{00} "local field effects" in the same spirit that Wiser[15] and Adler[16] have discussed dielectric constants.

The most time consuming part in Eq. (A6) involves inverting a $2N \times 2N$ matrix, while for Eq. (12) in the $k = 0$ limit, we need only to invert ϵ_{LL} which is an $N \times N$ matrix. Equation (12) is apparently more efficient. However, Eq. (A6) offers us some extra flexibility. There are two ways to obtain $\epsilon^{-1}_{K,K'}$: we can find the Fourier transform of the position dependent dielectric constant $\epsilon(r)$ first and then obtain the inverse of the matrix $\epsilon_{K,K'}$; or we can define the inverse function $1/\epsilon(r)$ before we perform the Fourier transform to obtain the matrix $\epsilon^{-1}_{K,K'}$. In the limit of large N, these two methods, which will be referred to as the inverse matrix and the inverse function method, respectively, have to converge to the same result. For finite N, the results can be different, reflecting truncation errors. The rate of convergence to the exact results will be different for these two methods. For Eqs. (9) and (12) given in this paper, ϵ^{-1}_{LL} corresponds to the inverse matrix method. The solution of Eq. (A6) will give the same result as Eq. (9) if we use the inverse matrix method.

We found that structures that support full photonic band gaps always form percolating networks of the high dielectric constant materials, and for these systems, the inverse matrix method converges much faster than the inverse function. Equation (12) is clearly best suited for these structures. There are, however, some exceptions, particularly for isolated material spheres that are close to touching, where the inverse function method converges faster than the inverse matrix method.[12] Although Eq. (A6) has to invert a matrix twice as large for a specified number of plane waves, there may be cases in which it can converge faster than Eq. (12) if the inverse function definition of $\epsilon^{-1}_{K,K'}$ is used. In Figs. 7(a) and 7(b), we plot the ϵ_{eff} vs $N^{-1/3}$ for a few situations we have considered, using both the closed-form E-field expression with the inverse matrix method [Eq. (12)] and Eq. (A6) using the inverse function method. We note that for the case of air spheres [Fig. 7(b)], the inverse matrix method [Eq. (12)] has much better convergence behavior than the inverse function method. For material spheres, Eq. (12) converges faster than the inverse function method for overlapping material spheres. For isolated material spheres near touching, such as the simple cubic structure at 50% filling ratio [the lower curves in Fig. 7(a)], we see that the inverse function method converges faster. In these cases, it may be better to obtain the effective dielectric constant using Eq. (A6). The results shown in Figs. 1 and 2 are obtained by the extrapolation procedure as depicted in Figs. 7(a) and 7(b).

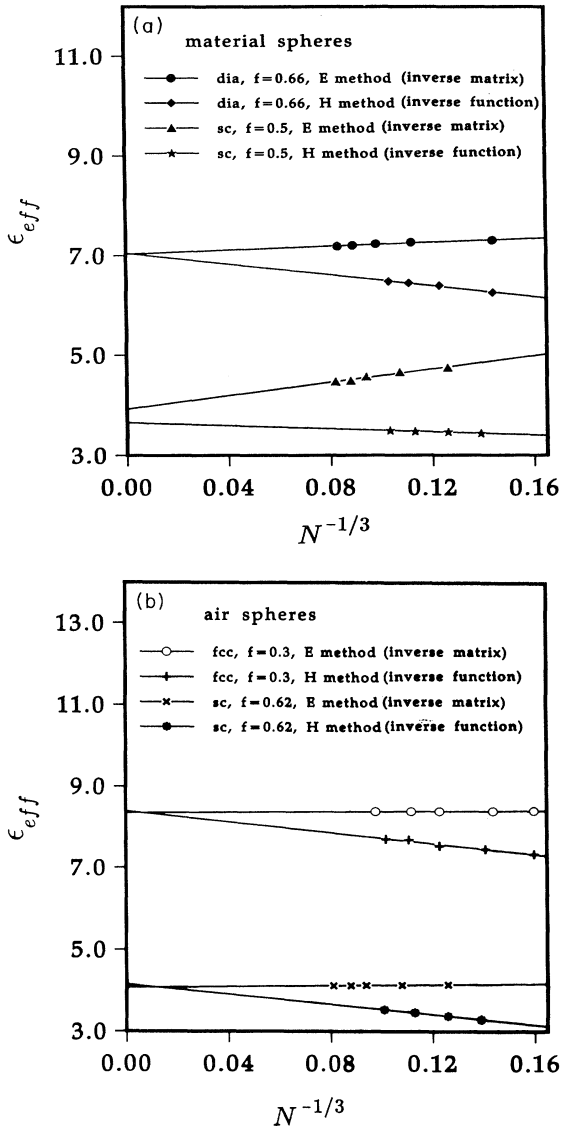

FIG. 7. (a) The effective dielectric constant ϵ_{eff} as a function of $N^{-1/3}$ for material spheres in air background. (b) The effective dielectric constant ϵ_{eff} as a function of $N^{-1/3}$ for air spheres in dielectric background.

[1]See, e.g., W. Lamb, D.M. Wood, and N.W. Ashcroft, Phys. Rev. B **21**, 2248 (1980).
[2]See, e.g., R. Landauer, in *Electrical Transport and Optical Properties of Inhomogeneous Media*, edited by J.C. Garland and D.B. Tanner, AIP Conf. Proc. No. 40 (AIP, New York, 1978).
[3]R.C. McPhedran and D.R. McKenzie, Proc. R. Soc. London Ser. A **359**, 45 (1978).
[4]R. Tao, Z. Chen, and P. Sheng, Phys. Rev. B **41**, 2417 (1990).
[5]L.C. Shen, C. Liu, J. Korringa, and K.J. Dunn, J. Appl. Phys. **67**, 7071 (1990).
[6]D.J. Bergman and K.J. Dunn, Phys. Rev. B **45**, 13 262 (1992).
[7]S. Satpathy, Z. Zhang, and M.R. Salehpour, Phys. Rev. Lett. **64**, 1239 (1990); **65**, 2478(E) (1990); **65**, 2650 (1990).
[8]K.M. Leung and Y.F. Liu, Phys. Rev. B **41**, 10 188 (1990); Phys. Rev. Lett. **65**, 2646 (1990).
[9]K.M. Ho, C.T. Chan, and C.M. Soukoulis, Phys. Rev. Lett. **65**, 3152 (1990); C.T. Chan, K.M. Ho, and C.M. Soukoulis, Europhys. Lett. **16**, 563 (1991); C.T. Chan, K.M. Ho, and C.M. Soukoulis, Mod. Phys. Lett. B **6**, 139 (1992).
[10]M. Plihal, A. Shambrook, A.A. Maradudin, and P. Sheng, Opt. Commun. **80**, 199 (1991).
[11]R.D. Meade, K.D. Brommer, A.M. Rappe, and J.D. Joannopoulos, Phys. Rev. B **44**, 10 961 (1991).
[12]H.S. Sözuer, J.W. Haus, and R. Inguva, Phys. Rev. B **45**, 13 962 (1992).
[13]E. Yablonovitch, Phys. Rev. Lett. **58**, 2059 (1987); E. Yablonovitch, T.J. Gmitter, and K.M. Leung, *ibid.* **67**, 2295 (1991).
[14]M. Born and E. Wolf, *Principles of Optics* (Pergamon, New York, 1980).
[15]N. Wiser, Phys. Rev. **129**, 62 (1963).
[16]S.L. Adler, Phys. Rev. **126**, 413 (1962).